

The Effect of Interior Stiffeners on the Flexural Behavior of Concrete-Filled Steel Tube Composite Box Girders

Hussam Aldin O. Abedi

Civil Engineering Department, Mustansiriya University, Iraq
hussamalsodany86@gmail.com

Mohammed M. Rasheed

Civil Engineering Department, Mustansiriya University, Iraq
mmrk72@uomustansiriya.edu.iq

Rusul Abed A. Alwaili

Civil Engineering Department, Mustansiriya University, Iraq
rusulalwaili88@gmail.com

Received: 3 June 2023 | Revised: 19 June 2023 and 23 June 2023 | Accepted: 29 June 2023

Licensed under a CC-BY 4.0 license | Copyright (c) by the authors | DOI: <https://doi.org/10.48084/etasr.6088>

ABSTRACT

The composite box girder is a structural element with high torsional stiffness and resistance against flexural loads. A new form of bridge construction is the Concrete-Filled Steel Tubes (CFSTs) linked to composite slabs by steel trusses. In this study, four different kinds of composite box girders linked to steel tubes filled with concrete were analyzed experimentally and numerically while being subjected to flexural loads. The specimens were evaluated when subjected to a focused load at the mid-span. The first model is a concrete-filled tube without stiffeners and was considered the control specimen, the second model is a concrete-filled tube with internal I-shaped stiffeners welded inside the steel tube, the third was filled with T-shaped stiffeners, and the fourth with V-shaped stiffeners. The test results showed that the CFST sections with interior stiffeners gave higher strength capacity and less deflection than the control specimen. The best shape of the stiffeners was the T-shape. The numerical analysis results were in accordance with the test results.

Keywords-composite box girder; concrete filled tubes; truss; flexural strength capacity; bridge analysis; finite element modeling; ABAQUS

I. INTRODUCTION

Composite bridges made from steel (girder) and concrete (slab) are the best way to reduce dead loads, such as the self-weight of the bridge. During the recent years, the composite bridges are constructed with top concrete slabs with steel trusses and bottom Concrete-Filled Steel Tubes (CFSTs). This type of bridge contains a large number of truss joints so there is stress concentration at these joints' location that reduces flexural capacity and may lead to failure [1]. The load-bearing structural system is served by the CFST composite trusses. While the shear force is converted into the axial force of the webs, the applied moment by the external load is converted into the axial forces of the upper and lower chords of the truss. The composite truss's chords are susceptible to axial force, thus the ideal approach is to fill the compressive chords with concrete due to its greater axial strength. In addition, the concrete core within the steel tube improves the buckling

behavior of the steel tubes. Additionally, the steel tube further encloses the concrete core [2].

The compressive strength of the slab and of the filled steel section (bottom chord), along with the geometry of the steel tube, have a significant impact on the behavior and strength capacity, crack propagation in the slab, deflection, and slip at the interface between the steel section and concrete, according to the experimental results of composite sections under the effect of concentrated load at the mid span of the top slab. While the load capacity and deflection are somewhat affected by the shear connections, the slip is more significantly affected [3]. The CFST section enhances the tensile strength by about 11% more than the steel section alone (hollow) [4]. CFST trusses with bracings for connections and a bottom chord filled with concrete are commonly used. The CFST enhances the flexural stiffness and joint strength of the truss as well as the compressive and tensile strength of the chords to prevent them from bowing inward and squeezing the lower chord's steel tube

(whole). The hollow steel section reduces the cost as it acts as a formwork for concrete casting [5-8].

In [9], a comparison was made between two kinds of trusses. The first truss was filled with concrete and the second truss was hollow. The strength capacity of the first member was 17.5% higher. In [10], six samples were tested with various girder trusses to examine the effects of the hollow upper and lower chords of the truss on the welded joints. According to the test findings, the inclusion of CFST chords boosted the joint's stiffness and load capacity, preventing the plastic failure of the chord's surface. In [11], eight specimens, including two hollow chord curved truss girders, four curved, and two straight CFST truss girders, were tested. The specimens' flexural behavior was examined without taking into account the height/span ratio and the presence of concrete infill. According to the test findings, curved CFST truss girders delivered greater stiffness and ultimate loads than straight CFST truss girders and curved hollow truss girders. In [12], four specimens were tested to explore the effect of the member's truss layout (diagonal and vertical) connected to lower and upper CFST members. Different modes of failure appeared, such as surface plasticity, local buckling, shear in the lower chord, and support failure. Authors in [13] investigated the flexural performance of CFST tube composite trusses considering different web configurations, such as transverse braces. According to the test findings, local buckling and surface plasticity at the bottom or the upper chord were the diagonal braces' failure modes. In comparison to the other specimens, the specimen with diagonal bracing exhibited better load capacity, stiffness, and ductility. The flexural strength of concrete girder enhanced by external structural materials due to prior damaged was studied in [14]. A bridge may fail due to the action of terrorist attacks such as explosives, so it is needed to make the bridge gliders strong enough [15], which damages the concrete girders [16].

According to the studies mentioned above, the research is limited in this area and more studies are needed to understand the behavior of such structures. The present study focuses on the influence of CFSTs on the flexural performance of composite box girders under static load. The effect of the presences stiffeners inside of CFST is also studied.

II. EXPERIMENTAL WORK

Four models of CFSTs which support concrete deck slabs are presented in this study. The model specimens include a control specimen and three specimens with different stiffener shapes welded along inside the CFST beam, as shown in Table I.

TABLE I. SPECIMEN MARKS AND DESCRIPTIONS

| Specimen | Description | Stiffener shape |
|----------|--|-----------------|
| B G | Composite tubular box girder filled with truss and concrete | Not applicable |
| B G W I | Composite tubular box girder filled with truss and concrete with I shaped stiffeners | I |
| B G W T | Composite tubular box girder filled with truss and concrete with T-shaped stiffeners | T |
| B G W V | Composite tubular box girder filled with truss and concrete with V-shaped stiffeners | V |

The geometry of the composite slabs, the connected truss, and CFSTs of all the tested specimens was the same except the shape of the interior stiffeners inside the CFST beam. The width of the specimens was 450 mm, the depth was 400 mm, and the total length was 2000 mm, in which the span from center to center between the supports was 1800 mm. The thickness of the concrete deck slabs was 100 mm. The trusses with 6 mm thickness were connected with the top concrete slabs by 8 mm thickness plates in which stud shear connectors were welded in above. The diameter of the stud shear connector was 12 mm distributed with center to center spacing of 100 mm. A steel tube with a thickness of 1.27 mm was used to fabricate the square tube cross-sections with outside depth and width of 150 mm. Based on selected dimensions, the width/thickness ratio is 118.11 so tube section was a slender section [17]. The steel tubes and the trusses were connected by weld connections. The three tested specimens had the same dimensions with the control specimen and differed only by the presence of the internal stiffeners with different shapes provided along the full length of each specimen. The steel stiffeners (I, T and V shaped) were separately fabricated and welded at their designed locations on a flat steel plate, after which, the plate was carefully folded by a press machine to achieve the suggested square shape of a cold-formed square steel tube. The square-shaped tube was fabricated by folding the flat steel plate into three folded sides. To complete the tube, the remaining face was formed by fully welding a flat steel plate onto the open edges along the already folded plate using a welding machine. The single stiffeners (along the span) were welded inside the steel tube as shown in Figure 1. Ordinary Portland Cement-Type I was cast in the concrete deck slabs and infill steel tubes. Its mechanical properties can be seen in Table II.

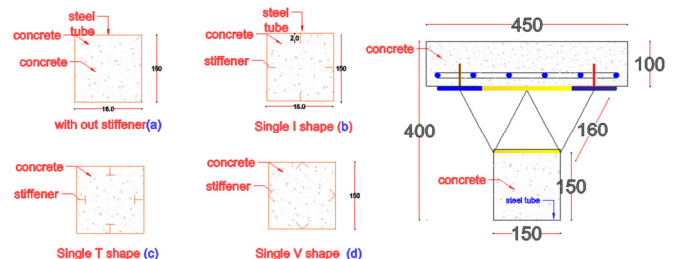


Fig. 1. Specimens details. (a) No stiffeners (BG), (b) I stiffeners (BGWI), (c) T stiffeners (BGWT), and (d) V stiffeners (BGWV).

TABLE II. MECHANICAL PROPERTIES OF CONCRETE (SLAB AND FILLED CONCRETE)

| Compressive strength f_c (MPa) | Modulus of rupture f_r (MPa) | Splitting tensile strength f_t (MPa) | Modulus of elasticity E_c (MPa) | Poisson ratio ν |
|----------------------------------|--------------------------------|--|-----------------------------------|---------------------|
| 30 | 3.337 | 4.244 | 25743 | 0.2 |

The above steel plates were connected with concrete deck slabs by shear connector studs. The geometry and specifications are listed in Tables III and IV, respectively. The concrete deck slab reinforcement and geometry are listed in Table V. The dimensions of the steel tubes and the filling concrete are listed in Table VI. The mechanical properties of

the main reinforcement of the slabs are listed in Table VII. Truss member properties and dimensions are listed in Table VIII.

TABLE III. SHEAR STUD CONNECTORS

| Diameter (mm) | Height (mm) | Spacing (mm) |
|---------------|-------------|--------------|
| 10 | 63.5 | 100 |

TABLE IV. MECHANICAL PROPERTIES OF SHEAR STUD CONNECTORS

| f_y (MPa) | E_s (MPa) | ν |
|-------------|-------------|-------|
| 412 | 200000 | 0.3 |

TABLE V. CONCRETE SLAB DETAILS

| Slab depth (mm) | Slab width (mm) | Main bottom reinforcement |
|-----------------|-----------------|----------------------------|
| 100 | 450 | Ø10@100 in both directions |

TABLE VI. STEEL TUBE AND FILLING CONCRETE DIMENSIONS

| Concrete Depth (mm) | Steel tube (mm) | | |
|---------------------|-----------------|--------------------------------|-----------|
| | Width (mm) | Depth and width-square section | Thickness |
| 150 | 150 | 150 | 1.27 |

TABLE VII. MECHANICAL PROPERTIES OF THE REINFORCEMENT

| Bar diameter (mm) | f_y (MPa) | Ultimate strength f_u (MPa) | E_s (MPa) | ν |
|-------------------|-------------|-------------------------------|-------------|-------|
| 10 | 487.67 | 660 | 200000 | 0.30 |

TABLE VIII. TRUSS MEMBER DIMENSIONS

| Type | Depth (mm) | Width (mm) | Thickness (mm) |
|---------|------------|------------|----------------|
| Channel | 25.4 | 50.8 | 6 |

Figure 2 shows the stud shear connector distribution along the deck slab welded to the upper steel plate, Figure 3 shows the deck slab reinforcement layout, Figure 4 shows the specimen setup and the strain gauges, in which two of them are located at the shear zone as ST1 and ST2 at each support's end while ST3 is located at the bottom center of each specimen. Central point load was applied up to failure in each specimen. The concentrated load was applied at the mid-span on the top surface of the deck slab. Strains and deflections were recorded for each load step and were then plotted.



Fig. 2. Stud shear connector distribution.



Fig. 3. Main reinforcements of the slab layout.

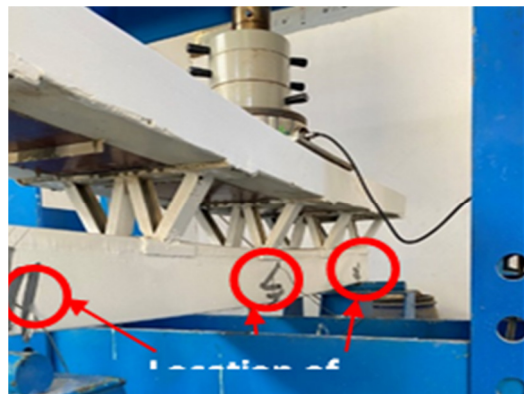


Fig. 4. Location of the strain gauges.

III. TEST RESULTS

In the current investigation, four specimens, including the control composite girder connected by steel truss to CFST without interior stiffeners and three specimens with different stiffeners were tested under concentrated load. The test results of are shown in Table IX.

TABLE IX. TEST RESULTS

| Model | Load capacity (kN) | Deflection at maximum load (mm) | Deflection at failure (mm) | Maximum strain | | |
|-------|--------------------|---------------------------------|----------------------------|-----------------------|-----------------------|-----------------------|
| | | | | ST1 X10 ⁻³ | ST2 X10 ⁻³ | ST3 X10 ⁻³ |
| BG | 168.70 | 15.53 | 16.88 | 1.3 | 1.06 | 0.071 |
| BGWI | 196.24 | 16.40 | 18.60 | 0.59 | 0.59 | 0.314 |
| BGWT | 220.53 | 24.00 | 28.51 | 0.57 | 0.54 | 0.560 |
| BG WV | 212.93 | 13.14 | 13.97 | 1.34 | 1.39 | 1.08 |

TABLE X. STIFFNESS AND DUCTILITY OF THE TESTED SPECIMENS

| Model | Increase of strength load capacity (%) | Deflection at the load of BG (mm) | Deflection decrease (%) | Stiffness (kN/mm) | Ductility |
|-------|--|-----------------------------------|-------------------------|-------------------|-----------|
| BG | --- | 15.53 | --- | 10.86 | 1.09 |
| BGWI | 16.32 | 10.87 | 30.01 | 11.96 | 1.13 |
| BGWT | 30.72 | 10.51 | 32.32 | 9.19 | 1.19 |
| BG WV | 26.22 | 8.03 | 48.29 | 16.20 | 1.06 |

The recorded strain values listed in Table IX for ST1 and ST2 are the same, but differ from ST3 which is located at the bottom center of the CFST beam. All strains were measured

with the limiting value recommended by ACI-318-2019 [18] which is less than 0.005. The stiffness and ductility of the tested specimens are listed in Table X. The stiffness was found by dividing the maximum strength capacity with the corresponding deflection and the ductility was the result of the division of the deflection at failure by the deflection at maximum load capacity. Specimen BGWV exhibits the highest stiffness while specimen BGWT the lowest. Specimen BGWT gave the highest ductility of 1.19 and specimen BGWV the lowest of 1.06 in.

The behavior and strength of the tested specimens are represented by the recorded load-deflection and load-strain relations for each applied load step. Figure 5 shows the load-deflection variations for the tested specimens. In general, the variation started as linear up to the inflection point. Thereafter, the specimens behave as nonlinear and their stiffness reduces. The inflection points differ in magnitude due to the differences in the connection of the unfilled concrete with the steel tube to form the CFST section. Specimen BGWV has the highest strength capacity with lowest deflection followed by BGWT, BGWI, and BG.

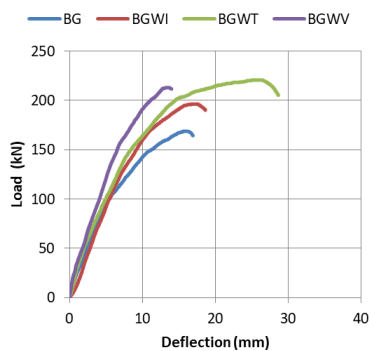


Fig. 5. Load-deflection relation of the tested specimens.

Figures 6 to 8 represent the load-strain variations of the tested specimens. ST1 and ST2 are the strains at the left and the right diagonal tension at the supports and ST3 represents the strain at the middle in the bottom of each specimen. The recorded strains ST1 and ST2 are almost equal. The strain of specimen BGWV was the lowest at the supports due to the connection stiffeners, followed by BGWI, BGWT, and BG. The strain ST3 of the control specimen BG was the lowest.

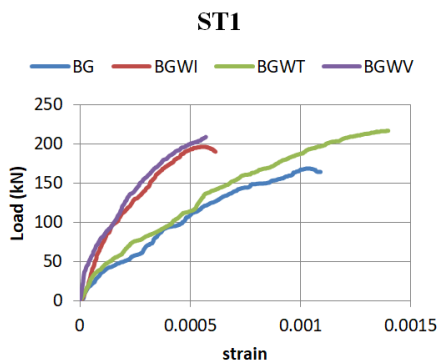


Fig. 6. Load-strain ST1 of the tested specimens.

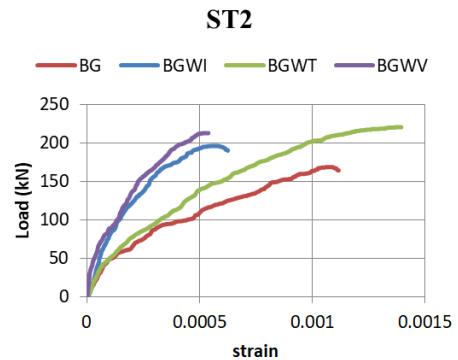


Fig. 7. Load-strain ST2 of the tested specimens.

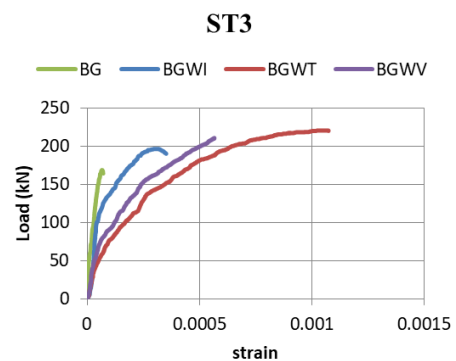


Fig. 8. Load-strain ST3 of the tested specimens.

IV. FINITE ELEMENT ANALYSIS

Element types were used to simulate the performance of CFSTs of composite box girders. The concrete element had 8 nodes. The truss element model had 2 nodes and the steel tube model shell element had 4. The contact between the concrete and bottom steel plate, concrete and with inner surface of the steel tube involved finite sliding with surface-to-surface formulation, which is the default method in ABAQUS for contact enforcement.

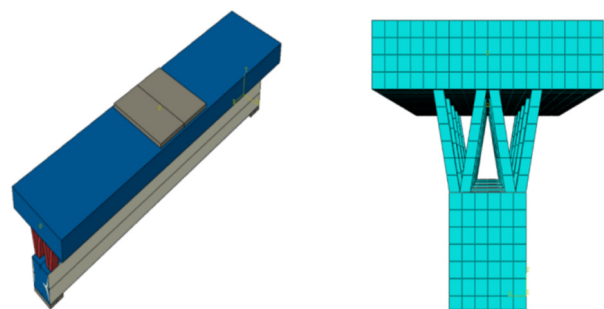


Fig. 9. Finite element model of the whole box girder.

The T3D2 with 2-node linear 3-D truss element was used to simulate reinforcements, stud shear connectors, and stiffeners. The shear stud connectors were simulated in such a manner that there would be no uplift failure so they can only be deformed horizontally due. The 4-node S4R doubly curved shell element was used to simulate the steel tube [19]. Figure 9 shows the finite element model simulation in ABAQUS.

Mainly, there are two material modeling approaches for concrete in ABAQUS, which are concrete smeared cracking and Concrete Damaged Plasticity (CDP) which is adopted in the present study. For the CDP model, in order to solve the Drucker-Prager plastic flow function and yield function, these parameters must be defined: dilation angle, form factor, eccentricity, bi-axial compressive stress ratio, dilation angle, and viscosity. The factors used to model the concrete are listed in Table XI.

TABLE XI. DAMAGE PLASTICITY DATA

| Damage plasticity data | | | | |
|------------------------|-----|-----------------|-------|-------|
| Dilation angle ϕ | e | f_{ho}/f_{co} | k | ν |
| 31 | 0.1 | 1.16 | 0.667 | 0 |

The stress-strain variation of concrete and steel are presented in Figures 10 and 11 respectively.

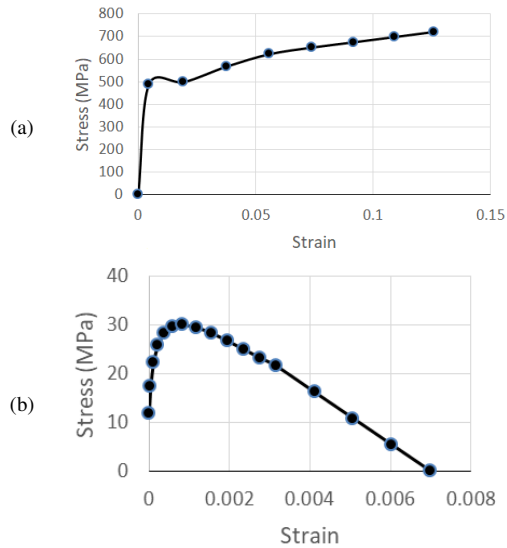


Fig. 10. Stress-strain variation of concrete: (a) Compression, (b) tension [20].

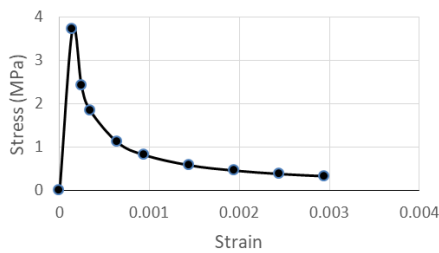


Fig. 11. Stress-strain variation of steel.

Figures 12-15 show the experimental and FEM analysis results of the load-mid span deflection for all specimens. The comparison shows a closeness in the results. Table XII lists the comparison analysis results. The finite element performance for all simulated models gave lower deflection than the experimental tests due to the rigid body of the model and the compatibility between the connected nodes of the elements. Figures 16-19 show the deflection of all models.

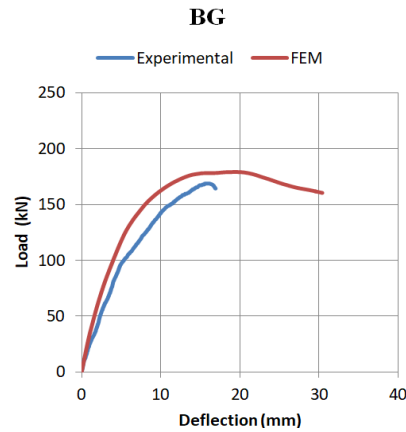


Fig. 12. Load-deflection relation of the experimental and FEM results for the BG specimen.

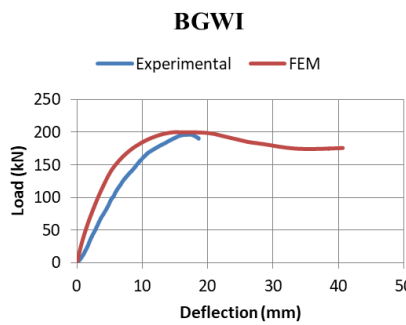


Fig. 13. Load-deflection relation of the experimental and FEM results for the BGWI specimen.

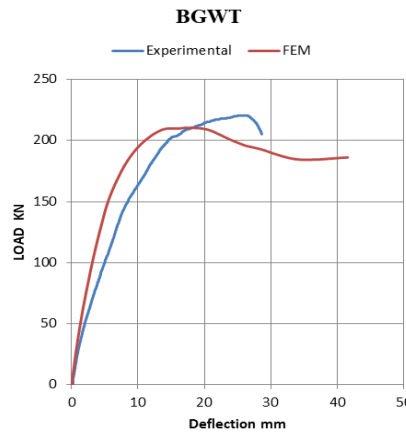


Fig. 14. Load-deflection relation of the experimental and FEM results for the BGWT specimen.

TABLE I. COMPARISON BETWEEN THE EXPERIMENTAL AND FEM ANALYSIS RESULTS

| Model | Load capacity (kN) | | Maximum deflection (mm) | | FEM/Experimental | |
|-------|--------------------|--------|-------------------------|-------|------------------|------------|
| | Experimental | FEM | Experimental | FEM | Load | Deflection |
| BG | 168.70 | 179.12 | 15.53 | 25.00 | 1.06 | 1.06 |
| BGWI | 196.24 | 200.00 | 16.4 | 15.00 | 1.01 | 0.90 |
| BGWT | 212.93 | 210.70 | 24 | 15.36 | 0.99 | 1.16 |
| BGWV | 220.53 | 210.50 | 13.14 | 19.20 | 0.95 | 0.80 |

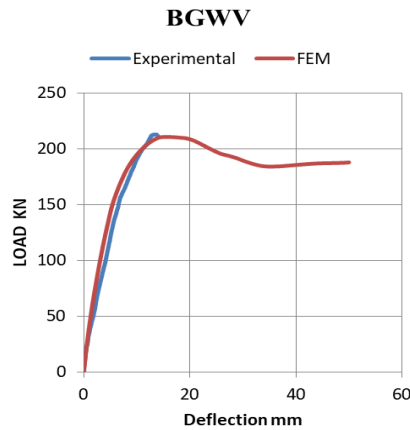


Fig. 15. Load-deflection relation of the experimental and FEM results for the BGWV specimen.

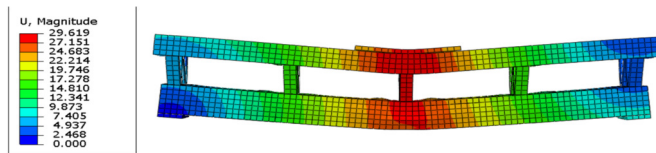


Fig. 16. Deflection of model BG at failure.

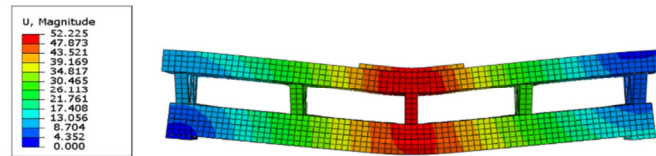


Fig. 17. Deflection of model BGWI at failure.

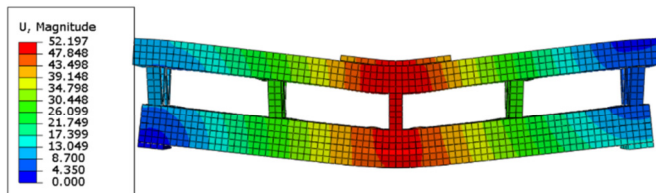


Fig. 18. Deflection of model BGWT at failure.

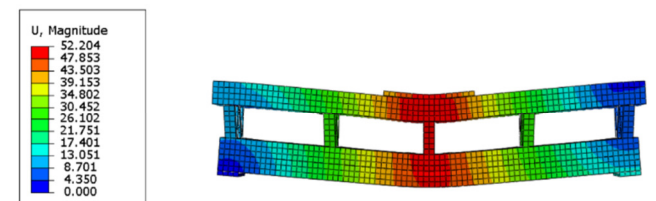


Fig. 19. Deflection of model BGWV at failure.

V. VON MISES STRESSES

The Von Mises stress were used to check out whether the adopted ductile material, i.e. steel, will yield or fracture. Figures 20-23 show the Von Mises stress distributions of all simulated models. The stress concentration occurs at the bottom of the CFST beam. Model BGWV exhibits the

minimum stress concentration and model BGWI the maximum. The Von Mises stress contours that represent the stress distributions show uniformity. The Von Mises maximum values ranged between 463 and 496 MPa, so the mean of the maximum value is more than the yield strength of the steel tube (383 MPa), so there is a fracture for all models at the failure stage.

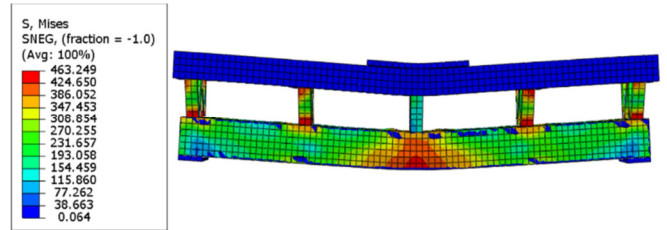


Fig. 20. Von Mises stresses of model BG at the final loading stage-FE results.

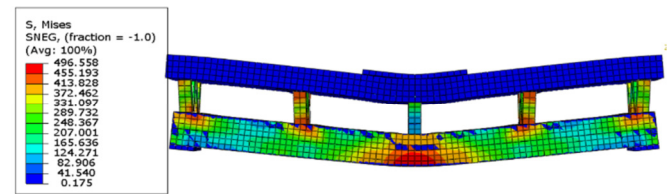


Fig. 21. Von Mises stresses of model BGWI at the final loading stage-FE results.

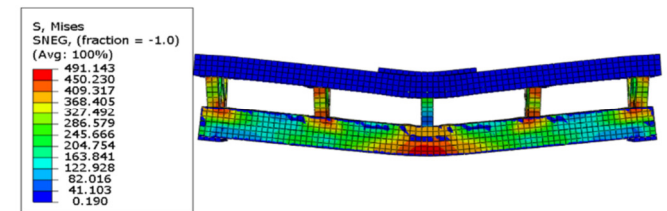


Fig. 22. Von Mises stresses of model BGWT at the final loading stage-FE results.

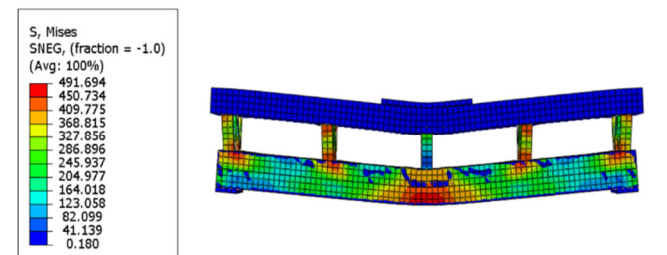


Fig. 23. Von Mises stresses of model BGWV at the final loading stage-FE results.

VI. DISCUSSION

The control specimen without interior stiffeners inside the CFST beam gave the lower strength capacity due to the absence of stiffeners, leading to a lack of interaction and a slip development between the steel tube and the filled concrete. In this case, the resistance force was only the frictional tube (adhesive) between the concrete and the steel section. Maximum strength capacity occurs in the case of T-shaped

stiffeners due to their resistance to the shear flow developed at the interface between the concrete and the steel tube. The other specimens, with I and V stiffeners, gave higher strength capacity than the control BG but less than BGWT. The deflection of specimen BGWT was less than control's and the specimens that used different stiffener shapes acquired more composite action while the flange of the stiffeners gave higher resistance to the composite bottom chord. The results of the finite element analysis were close with the experimental ones, giving less deflection due to the rigid body between the connected nodes of the elements. The number of shear stud connectors with full interaction between the steel plate and the deck reinforced concrete slab that lead the slip at the interface becomes very small or vanishes. No uplift failure occurred between the steel plate and the concrete deck slab in the experiments and finite element modeling.

VII. CONCLUSIONS

Based on the test and finite element analysis results of the four considered concrete filled steel tube box girders under flexural loads, the following conclusions can be reported:

- The strength capacity of the composite girders connected by trusses to the filled steel tubes at the bottom chord depends on the presence of interior stiffeners. The presence of interior stiffeners increases the bond between the concrete and the interior face of the CFSTs, making the concrete and the steel tube to work as a unity (full interaction) so that there is no slip, therefore the deflection become less and the strength capacity becomes higher and the developed flexural stress (bending stress) is reduced.
- The strength capacity of composite girders depends on the shape of the stiffeners. The T-shaped stiffeners gave higher strength capacity than the other types.
- Deflection and strain become less in the presence of stiffeners because there is no slip between the inside concrete and the hollow steel tube.
- The interior stiffeners increase the strength capacity and ductility, so they delay the occurrence of failure and prevent large deformations.
- Interior stiffeners improved the strength capacity of the tubes, meaning that the stiffeners improve the concrete confinement effects.

REFERENCES

- [1] Y. Chen, J. Dong, and T. Xu, "Composite box girder with corrugated steel webs and trusses – A new type of bridge structure," *Engineering Structures*, vol. 166, pp. 354–362, Jul. 2018, <https://doi.org/10.1016/j.engstruct.2018.03.047>.
- [2] Z. Tian, Y. Liu, L. Jiang, W. Zhu, and Y. Ma, "A review on application of composite truss bridges composed of hollow structural section members," *Journal of Traffic and Transportation Engineering (English Edition)*, vol. 6, no. 1, pp. 94–108, Feb. 2019, <https://doi.org/10.1016/j.jtte.2018.12.001>.
- [3] K. M. Alnebbhan and M. A. Shallal, "Composite concrete and concrete filled steel tube (CFST) truss girders," *Structural Integrity and Life*, vol. 20, no. 2, pp. 103–112, 2020.
- [4] L.-H. Han, S.-H. He, and F.-Y. Liao, "Performance and calculations of concrete filled steel tubes (CFST) under axial tension," *Journal of Constructional Steel Research*, vol. 67, no. 11, pp. 1699–1709, Nov. 2011, <https://doi.org/10.1016/j.jcsr.2011.04.005>.
- [5] W. Huang, Z. Lai, B. Chen, Z. Xie, and A. H. Varma, "Concrete-filled steel tube (CFT) truss girders: Experimental tests, analysis, and design," *Engineering Structures*, vol. 156, pp. 118–129, Feb. 2018, <https://doi.org/10.1016/j.engstruct.2017.11.026>.
- [6] Z. Lai and A. H. Varma, "Noncompact and slender circular CFT members: Experimental database, analysis, and design," *Journal of Constructional Steel Research*, vol. 106, pp. 220–233, Mar. 2015, <https://doi.org/10.1016/j.jcsr.2014.11.005>.
- [7] Z. Lai, A. H. Varma, and L. G. Griffis, "Analysis and Design of Noncompact and Slender CFT Beam-Columns," *Journal of Structural Engineering*, vol. 142, no. 1, Jan. 2016, Art. no. 04015097, [https://doi.org/10.1061/\(ASCE\)ST.1943-541X.0001349](https://doi.org/10.1061/(ASCE)ST.1943-541X.0001349).
- [8] Z. Lai, A. H. Varma, and K. Zhang, "Noncompact and slender rectangular CFT members: Experimental database, analysis, and design," *Journal of Constructional Steel Research*, vol. 101, pp. 455–468, Oct. 2014, <https://doi.org/10.1016/j.jcsr.2014.06.004>.
- [9] S.-L. Chan and M. Fong, "Experimental and analytical investigations of steel and composite trusses," *Advanced Steel Construction*, vol. 7, no. 1, pp. 17–26, Mar. 2011, <https://doi.org/10.18057/UASC.2011.7.1.2>.
- [10] W. Huang, L. Fenu, B.-C. Chen, J. Liu, and B. Briseghella, "Resistance of Welded Joints of Concrete-filled Steel Tubular Truss Girders," in *10th International Conference on Advances in Steel Concrete Composite and Hybrid Structures*, Singapore, Jan. 2012, pp. 547–554, https://doi.org/10.3850/978-981-07-2615-7_067.
- [11] W. Xu, L.-H. Han, and Z. Tao, "Flexural behaviour of curved concrete filled steel tubular trusses," *Journal of Constructional Steel Research*, vol. 93, pp. 119–134, Feb. 2014, <https://doi.org/10.1016/j.jcsr.2013.10.015>.
- [12] Y. Chen, R. Feng, and S. Gao, "Experimental study of concrete-filled multiplanar circular hollow section tubular trusses," *Thin-Walled Structures*, vol. 94, pp. 199–213, Sep. 2015, <https://doi.org/10.1016/j.tws.2015.04.013>.
- [13] B. Hu and J. Wang, "Experimental investigation and analysis on flexural behavior of CFSTTC beams," *Thin-Walled Structures*, vol. 116, pp. 277–290, Jul. 2017, <https://doi.org/10.1016/j.tws.2017.03.024>.
- [14] H. Q. Abbas and A. H. Al-Zuhairi, "Flexural Strengthening of Prestressed Girders with Partially Damaged Strands Using Enhancement of Carbon Fiber Laminates by End Sheet Anchorages," *Engineering, Technology & Applied Science Research*, vol. 12, no. 4, pp. 8884–8890, Aug. 2022, <https://doi.org/10.48084/etasr.5007>.
- [15] B. F. Abdulkareem, A. F. Izzet, and N. Oukaili, "Post-Fire Behavior of Non-Prismatic Beams with Multiple Rectangular Openings Monotonically Loaded," *Engineering, Technology & Applied Science Research*, vol. 11, no. 6, pp. 7763–7769, Dec. 2021, <https://doi.org/10.48084/etasr.4488>.
- [16] H. M. Hekmet and A. F. Izzet, "Performance of Segmental Post-Tensioned Concrete Beams Exposed to High Fire Temperature," *Engineering, Technology & Applied Science Research*, vol. 9, no. 4, pp. 4440–4447, Aug. 2019, <https://doi.org/10.48084/etasr.2864>.
- [17] *ANSI/AISC 360-16 Specification for Structural Steel Buildings*. Chicago, IL, USA: AISC, 2016.
- [18] ACI Committee 318, *318-19 Building Code Requirements for Structural Concrete and Commentary*. Farmington Hills, MI, USA: American Concrete Institute, 2019.
- [19] "Abaqus 6.14 Documentation." <http://130.149.89.49:2080/v6.14/>.
- [20] J. B. Mander, M. J. N. Priestley, and R. Park, "Theoretical Stress-Strain Model for Confined Concrete," *Journal of Structural Engineering*, vol. 114, no. 8, pp. 1804–1826, Sep. 1988, [https://doi.org/10.1061/\(ASCE\)0733-9445\(1988\)114:8\(1804\)](https://doi.org/10.1061/(ASCE)0733-9445(1988)114:8(1804)).